European Journal of Chemistry 8 (4) (2017) 349-357

European Journal of Chemistry

Journal webpage: www.eurjchem.com

Molecular self-assembly in indole-based benzamide derivative: Crystal structure, Hirshfeld surfaces and antimicrobial activity

Ilkay Gumus [1,*], Ummuhan Solmaz [1], Serpil Gonca [2] and Hakan Arslan [1]

[1] *Department of Chemistry, Faculty of Arts and Science, Mersin University, Mersin, TR 33343, Turkey*
[2] *Department of Pharmaceutical Microbiology, Faculty of Pharmacy, Mersin University, Mersin, TR 33343, Turkey*

** Corresponding author at: Department of Chemistry, Faculty of Arts and Science, Mersin University, Mersin, TR 33343, Turkey. Tel.: +90.324.3610001/14559. Fax: +90.324.3610047. E-mail address: ilkay.gumus@mersin.edu.tr (I. Gumus).*

ARTICLE INFORMATION

DOI: 10.5155/eurjchem.8.4.349-357.1637

Received: 12 October 2017
Received in revised form: 28 October 2017
Accepted: 28 October 2017
Published online: 31 December 2017
Printed: 31 December 2017

KEYWORDS

Antimicrobial activity
Single crystal structure
Molecular self-assembly
Hirshfeld surface analysis
Deformation electron density
Indole-based benzamide derivative

ABSTRACT

Two new compounds, 1*H*-indole-7-amine (1) and *N*-(1*H*-indol-7-yl)-2-methylbenzamide (2) were synthesized and structurally characterized by NMR and FT-IR spectroscopic techniques. The molecular structure of compound 2 was further elucidated by single-crystal X-ray diffraction technique. Moreover, the crystal packing of compound 2 is analyzed in terms of non-covalent N-H···O, C-H···π, and parallel displaced π···π interactions. Hirshfeld surface analysis and decomposed fingerprint plots of the compound 2 were performed to visualize the presence of strong hydrogen bond N-H···O and C-H···π stacking interactions. Hirshfeld surface analysis and decomposed fingerprint plots show that the structure of compound 2 is stabilized by H···H, N-H···O, C-H···π and π···π intermolecular interactions and these interactions contribute mostly to molecular self-assembly in the crystal. In addition, compound 2 was evaluated for both their *in-vitro* antibacterial and antifungal activity. The obtained results have been reported, explained and compared with fluconazole and ampicillin used as reference drugs.

Cite this: *Eur. J. Chem.* **2017**, *8(4)*, 349-357

1. Introduction

The indole nucleus is a planar bicyclic molecule containing 10-π electrons and it is aromatic compound according to Hückel's rule [1]. Chemically, this heterocyclic ring system is a fusion of six-membered benzene and five-membered pyrrole ring [2,3]. The indoles are privileged molecules in the chemical literature due to their diverse biological properties and found in a number of natural products and bioactive molecules [4-8]. Indole derivatives are an important class of therapeutic agents in medicinal chemistry [9,10]. The various activities associated with them include analgesic [5] antiallergic [11], antibacterial [9], antitumor [10], anti HIV [12], antioxidant [13], and anti-rheumatoid activities [10]. Some of the indole analogues also inhibit development of bladder cancer, cell carcinoma, lung cancer, colon cancer, mammary tumors, prostate cancer, and breast tumor cells [14,15]. In addition, many substituted indoles are possessing redox active properties, potent scavengers of free radicals and are able to bind many receptors with high affinity [5,14,16]. The indole ring is capable of various noncovalent interactions with other molecules by hydrogen bonding through the NH moiety and by π···π stacking, cation···π interactions, etc., through the aromatic moiety [17]. The study of indole inter- and intra-molecular interactions is essential for better understanding of its reactivity and mechanism of interactions in biological systems [18]. The noncovalent and weak interactions with the surrounding groups may also affect the binding properties and redox potential of the metal center in their complexes [19,20-22].

Owing to the importance of biologically, physiologically and pharmaceutically active indole compounds, we focused on the investigation of the molecular structure of indole-based benzamide derivative. In our work, 1*H*-indole-7-amine (**1**) and *N*-(1*H*-indol-7-yl)-2-methylbenzamide (**2**) were synthesized and structurally characterized by NMR and FT-IR spectroscopic techniques. The crystal structure and conformational properties of synthesized compound **2** have been also determined *via* single crystal X-ray diffraction studies. The intermolecular contacts in compound **2** have been performed based on the Hirshfeld surfaces and their associated 2D fingerprint plots.

2. Experimental

2.1. Instrumentation

Carbon, hydrogen and nitrogen analyses were carried out on a Carlo Erba MOD 1106 elemental analyzer.

ISSN 2153-2249 (Print) / ISSN 2153-2257 (Online)
http://dx.doi.org/10.5155/eurjchem.8.4.349-357.1637

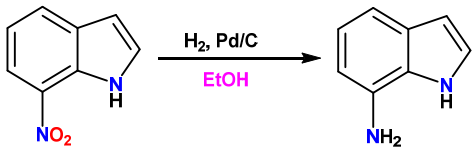

Scheme 1

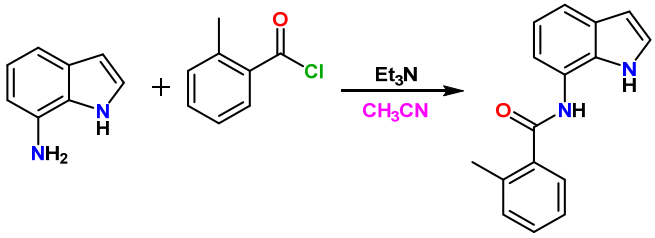

Scheme 2

Infrared measurement was recorded in the range 400-4000 cm^{-1} on a Perkin Elmer Spectrum 100 series FT-IR/FIR/NIR Spectrometer Frontier, ATR Instrument. The NMR spectra were recorded in DMSO-d_6 solvent on Bruker Avance III 400 MHz NaNoBay FT-NMR spectrophotometer using tetramethylsilane as an internal standard.

The X-ray diffraction data were recorded on a Bruker APEX-II CCD diffractometer. A suitable crystal was selected and coated with Paratone oil and mounted onto a Nylon loop on a Bruker APEX-II CCD diffractometer. The crystal was kept at T = 100 K during data collection. The data were collected with MoKα (λ = 0.71073 Å) radiation at a crystal-to-detector distance of 40 mm. Using Olex2 [23], the structure was solved with the Superflip [24-26] structure solution program, using the Charge Flipping solution method and refined by full-matrix least-squares techniques on F^2 using ShelXL [27] with refinement of F^2 against all reflections. Hydrogen atoms were constrained by difference maps and were refined isotropically, and all non-hydrogen atoms were refined anisotropically. The molecular structure plots were prepared using PLATON [26]. The anisotropic thermal parameters and structure factors (observed and calculated), full list of bond distances, bond angles and torsional angles are given in supplementary materials. The geometric special details: all e.s.d.'s (except the e.s.d. in the dihedral angle between two l.s. planes) are estimated using the full covariance matrix. The cell e.s.d.'s are taken into account individually in the estimation of e.s.d.'s in distances, angles and torsion angles; correlations between e.s.d.'s in cell parameters are only used when they are defined by crystal symmetry. An approximate (isotropic) treatment of cell e.s.d.'s is used for estimating e.s.d.'s involving l.s. planes.

2.2. Synthesis and characterization

The 7-nitroindole is commercially available and purchased from Sigma Aldrich. *o*-Toluoyl chloride, Pd/C (%5) and triethylamine were purchased from Merck and used as received. All other chemicals and solvents were obtained from commercial suppliers and used without further purification.

2.2.1. Synthesis of 1H-indole-7-amine (1)

1*H*-Indole-7-amine (**1**) was prepared according to previously published method [28]. 7-Nitroindole (1.1 g, 6.8 mmol) was dissolved in ethanol (50 mL) and 5% palladium on charcoal was added (0.2 g). The mixture was vigorously stirred under hydrogen atmosphere. The catalyst was filtered off on Celite about 2 hours. The solvent was evaporated, and the solid residue was recrystallized from dichloro-methane:*n*-hexane (1:5, *v*:*v*) (Scheme 1). Color: Colorless. Yield: 75%. FT-IR (ATR, ν, cm^{-1}): 3377, 3306 ν(N-H) (w), 3056, 3024 ν(Ar-CH) (w). ^{1}H NMR (400 MHz, DMSO-d_6, δ, ppm): 10.64 (s, 1H, NH), 7.25 (t, 1H, Ar-H), 6.76 (m, 2H, Ar-H), 6.35 (d, 1H, Ar-H), 6.31 (t, 1H, Ar-H), 5.01 (s, 2H, NH_2). ^{13}C NMR (100 MHz, DMSO-d_6, δ, ppm): 134.2, 128.7, 126.1, 124.2, 120.4, 109.1, 105.1, 102.0. Anal. calcd. for $C_8H_8N_2$: C, 72.70; H, 6.10; N, 21.20. Found: C, 72.10; H, 6.01; N, 21.02 %.

2.2.2. Synthesis of N-(1H-indol-7-yl)-2-methylbenzamide (2)

1*H*-Indole-7-amine (0.5 g, 3.8 mmol) was added to a 100 mL two necked round-bottomed flask equipped with a magnetic stirrer. The flask was closed with a septum and purged with nitrogen gas. Afterwards, freshly dried CH_3CN (50 mL) and triethylamine (0.580 mL, 4.18 mmol) were added with a syringe. After cooling the reaction mixture to -30 °C, *o*-toluoyl chloride (0.543 mL, 4.18 mmol) was slowly added dropwise. Then, the suspension was allowed to achieve room temperature and stirred overnight. When the reaction was finished, the precipitated product was filtered off, and purified by crystallization from dichloromethane:*n*-hexane (1:5, *v*:*v*) (Scheme 2). Color: Colorless. Yield: 69%. FT-IR (ATR, ν, cm^{-1}): 3256 ν(N-H) (w), 3070, 3030 ν(Ar-CH) (w), 2917 ν(CH_3) (w), 1636 ν(C=O) (s). ^{1}H NMR (400 MHz, DMSO-d_6, δ, ppm): 10.80 (s, 1H, NH), 10.04 (s, 1H, NH), 7.58 (q, 2H, Ar-H), 7.36 (m, 5H, Ar-H), 6.99 (t, 1H, Ar-H), 6.47 (q, 1H, Ar-H), 2.44 (s, 3H, CH_3). ^{13}C NMR (100 MHz, DMSO-d_6, δ, ppm): 161.2, 141.1, 136.2, 133.4, 132.0, 130.2, 128.9, 127.8, 124.3, 122.5, 120.9, 118.1, 113.2, 103.1, 18.9. Anal. calcd. for $C_{16}H_{14}N_2O$: C, 76.78; H, 5.64; N, 11.19. Found: C, 75.61; H, 5.64; N, 11.10 %.

2.3. Hirshfeld surfaces analysis

Analysis of Hirshfeld surfaces and their associated two-dimensional fingerprint plots of compound **2** were calculated using Crystal Explorer 3.1 [29]. The Hirshfeld surfaces mapped with different properties d_{norm}, shape index, d_i and d_e. The d_{norm} is normalized contact distance, defined in terms of d_e, d_i and the vdW radii of the atoms. Deformation density is generated from Crystal Explorer3.1, over the electron density iso-surface (the value is 0.008 e/au^3) using HF method with 6-31G(d) as basis set.

2.4. Antimicrobial activity studies

Antimicrobial susceptibility testing was performed by modification microdilution of the following literature methods [30,31].

Table 1. Crystal data and details of the structure refinement for compound **2**.

Parameters	Compound 2
Empirical formula	$C_{16}H_{14}N_2O$
Formula weight	250.29
Temperature (K)	116.42
Crystal system	Orthorhombic
Space group	$Pca2_1$
a, (Å)	8.2877(11)
b, (Å)	7.5482(9)
c, (Å)	20.041(2)
Volume (Å^3)	1253.7(3)
Z	4
ρ_{calc} (g/cm^3)	1.326
μ (mm^{-1})	0.084
F(000)	528.0
Crystal size (mm^3)	0.24 × 0.13 × 0.09
Radiation	MoKα (λ = 0.71073)
2Θ range for data collection (°)	6.758 to 53.706
Index ranges	$-10 \le h \le 10$, $-9 \le k \le 9$, $-25 \le l \le 21$
Reflections collected	14634
Independent reflections	2525 [R_{int} = 0.1724, R_{sigma} = 0.1163]
Data/restraints/parameters	2525/1/173
Goodness-of-fit on F^2	1.098
Final R indexes [I≥2σ (I)]	R_1 = 0.0666, wR_2 = 0.0988
Final R indexes [all data]	R_1 = 0.1230, wR_2 = 0.1115
Largest diff. peak/hole (e Å^{-3})	0.24/-0.26
Flack parameter	-0.6(10)

We used microbial strains such as *Staphylococcus aureus* (ATCC 25923), *Streptococcus pneumonia* (ATCC 6303), *Escherichia coli* (ATCC 35218), *Pseudomonas aeruginosa* (ATCC 27853), *Acinetobacter baumannii* (RSHM 2026), *Candida albicans* (ATCC 10231) and *Candida glabrata* (RSHM 40199).

The fungal and bacterial cell inoculums were prepared from the stock culture grown in Tryptic Soy Agar (TSA) at 28 °C for 24 h and Mueller-Hinton Agar (MHA) 37 °C for 24 h, respectively. The microorganism suspension concentrations were adjusted according to McFarland 0.5 turbidity tubes using sterilized saline. Stock solution of title compound was prepared in DMSO at 1000 μg/mL. A modified microdilution test was applied for antimicrobial activity and the experiments were run in duplicates independently.

For antifungal activity testing, 100 μL Tryptic Soy Broth (TSB) was added to each of 11 well. 100 μL of chemical derivative solution was added to the first well and 2-fold dilutions were prepared. Then, 5 μL of fungal suspension was added to each tube except the last one which acted as a control well.

For antibacterial activity testing, 100 μL Mueller-Hinton Broth (MHB) was added to each of 11 well. 100 μL of chemical derivative solution was added to the first tube and 2-fold dilutions were prepared. Then, 5 μL of the bacterial suspension was added to each tube except the last control well. Only 5 μL of fungal and bacterial suspension were added in another to control tube without chemical and used as control for growing. All plates were incubated at 28 °C (for fungi) and at 37 °C (for bacteria) for 24 h. After the incubation, the minimal inhibitory concentrations (MIC) were noted by controlling the growth inhibition for title compound. Fluconazole and ampicillin were used as reference drug. The results were read visually and by measuring optical density for 24 h.

3. Result and discussion

3.1. Spectral characterization

Indole-7-amine (**1**) was simply obtained by the catalytic reduction (H_2, Pd/C 5%) of 7-nitroindole, which is comercially available. The amide-based compound **2** was obtained by reactions of the corresponding *o*-methyl benzoyl chloride with indolyl-7-amine and characterized by FT-IR, ^{1}H NMR and ^{13}C NMR spectroscopic technique. The crystal structure of compound **2** was elucidated by single crystal X-ray diffraction technique. The FT-IR and NMR data confirmed the presence of both compounds.

The compound **1** shows characteristic peaks in FT-IR due to ν(NH_2) and ν(N-H) stretching vibration at 3377 and 3306 cm^{-1}, respectively. In the FT-IR spectrum of the compound **2**, disappearance of these two signals and the appearance of new band at 3256 cm^{-1}, corresponding to the stretching of the amide group, confirmed the formation of the compound **2**. Also, the band at 3070-3030 and 1636 cm^{-1} correspond to stretching of ν(C_{sp^2}-H) and ν(C=O) groups of compound **2**, respectively.

The compound **1** is easily identified by ^{1}H NMR spectra by the presence of resonances at δ 10.64 ppm for the NH-pyrrole proton and δ 5.01 ppm for -NH_2 protons. The resonance values of these signals shifted to downfield (Δδ ~0.16 ppm for NH-pyrrole and Δδ ~5.03 ppm NH-CO) in the ^{1}H NMR spectrum of the compound **2**. The signals for the aromatic protons in the compound **1** were observed in the range of δ 7.25-6.31 ppm while the aromatic protons signals for the compound **2** were observed in the range of δ 7.58-6.47 ppm. Also, a new singlet peak at δ 2.44 ppm seen in ^{1}H NMR spectrum of compound **2** corresponds to CH_3 group. Meanwhile, the ^{13}C NMR spectrum of compound **2** shows expected carbon signals. The peaks at δ 161.2 and 18.9 ppm correspond to the carbonyl carbon of the amide group and methyl carbon, respectively.

3.2. Crystal structure analysis

A suitable single crystal of compound **2** for X-ray diffraction study was obtained by slow evaporation of a dichloromethane:*n*-hexane (1:5, *v*:*v*) solution. Crystallographic data and refinement parameters are summarized in Table 1 and selected bond parameters are tabulated in Table 2.

Compound **2** crystallizes in $Pca2_1$ space group with one molecule in the asymmetric unit. Figure 1 shows the molecular structure and the atom-labeling scheme of compound **2**. The C=O bond length is 1.245(5) Å and this bond length is found in the range of typical double bonds for C=O groups [32]. The C-N bond lengths for the compound **2** are all shorter than the average single C–N bond length of 1.48 Å, being N1-C1 = 1.346(6), N1-C9 = 1.439(6), N2-C15 = 1.376(6) and N2-C16 = 1.373(6) Å, thus showing varying degrees of double bond character in these C-N bonds. Also, the sum of the angles around the indole nitrogen reveals the expected nearly ideal sp^2-hybridization with 358.8° value.

Table 2. Selected bond lengths (Å), bond and torsion angles (°) of compounds **2**.

Atom		Length (Å)	Atom			Angle (°)	Atom				Angle (°)
O1	C1	1.245(5)	C10	C9	N1	123.1(4)	O1	C1	C2	C3	-132.7(5)
N1	C1	1.346(6)	C10	C9	C16	118.2(4)	O1	C1	C2	C7	43.6(7)
N1	C9	1.439(6)	C16	C9	N1	118.7(4)	N1	C1	C2	C3	44.6(6)
N2	C15	1.376(6)	N2	C16	C9	130.3(4)	N1	C1	C2	C7	-139.0(4)
N2	C16	1.373(6)	N2	C16	C13	108.4(4)	N1	C9	C10	C11	179.0(4)
C1	C2	1.495(6)	C9	C16	C13	121.3(4)	N1	C9	C16	N2	3.1(7)
C2	C3	1.394(6)	O1	C1	N1	123.3(4)	N1	C9	C16	C13	-177.4(4)
C2	C7	1.410(6)	O1	C1	C2	121.8(4)	C1	N1	C9	C10	41.7(7)
C3	C4	1.377(7)	N1	C1	C2	114.9(4)	C1	N1	C9	C16	-139.9(5)
C4	C5	1.386(7)	C1	N1	C9	125.1(4)	C1	C2	C3	C4	175.1(4)

Table 3. Intra-and inter-molecular hydrogen bonds for compounds **2** (Å, °).

D-H···A	d(D-H)	d(H···A)	d(D···A)	∠(D-H···A)	Symmetry
C10-H10···O1	0.94	2.61	2.995	105	-
C8-H8B···O1	0.98	2.66	2.946	91	-
C8-H8C···O1	0.98	2.79	2.94	90.4	-
N1-H1···O1	0.88	2.055	2.878	155.03	1/2+*x*, 1-*y*, +*z*
N2-H2···O1	0.88	2.179	2.910	140.20	1/2+*x*, 1-*y*, +*z*

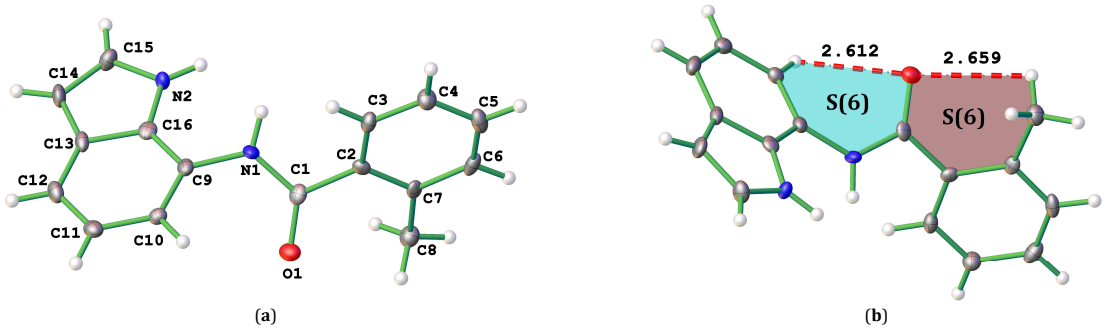

(**a**) (**b**)

Figure 1. (**a**) Molecular structure of the compound **2**, showing the atom-numbering scheme (**b**) The intramolecular hydrogen bonds cause the formation of the two fused S(6) ring motif in compound **2**.

The planar indole ring is almost perpendicular to the phenyl ring attached to the carbonyl group with the dihedral angle of 87.02(4)°.

The crystal packing of compound **2** is stabilized by a combination of intramolecular and intermolecular hydrogen bonds, C-H···π and π···π stacking interactions (Table 3). The intramolecular C_{sp^3}-H···O 2.66 Å and C_{sp^2}-H···O 2.61 Å hydrogen bonds cause the formation of a fused two six-membered ring system S(6) in each crystal structure (Figure 1b).

In compound **2**, strong intermolecular N-H···O interactions occur. In this interaction, the carbonyl oxygen O1 atom in the molecule acts as an acceptor to the amide and indole nitrogen of the partner molecule (Figure 2). Thus, strong N_{amide}-H···O and N_{indol}-H···O hydrogen bonds were observed to connect the molecules in the formation of the supramolecular chain along the crystallographic [010] direction (Figure 2a).

The supramolecular chain was also supported by C_{sp^2}-H···$\pi_{pyrrole}$ and C_{sp^2}-H···$\pi_{benzene}$ stacking interactions along the same crystallographic direction (Figure 2b). The methyl substituent in *o*-position of compound **2** leads to intermolecular C_{sp^3}-H···π stacking interactions and each supramolecular chain is interconnected *via* these C_{sp^3}-H···π interactions (Figure 3). Also, it is interesting to note that both, the C_{sp^3}-H···π and N-H···O intermolecular interactions, lead to infinite one dimension helical chains of compound **2** along the [001] direction (Figure 2d).

In addition, the crystal structure is further stabilized by intermolecular π···π stacking interactions, leading to zigzag chains along [101] and [001] directions (Figure 4). This π···π stacking mode can be defined as a parallel-displaced arrangement. The intermolecular parallel-displaced π···π interactions with dominating π···σ attraction occur between the indole rings in the two neighboring molecules [33]. The parallel-displaced π···π interactions between the pyrrole rings of indole are stronger than the parallel-displaced π···π interactions between the benzene rings and so they contribute to structure stabilization (Table 4).

3.3. Hirshfeld surfaces analysis

The Hirshfeld surface analysis provides understanding of intermolecular interactions in forming supramolecular structure. The intermolecular interactions in crystal structure of compound **2** have been examined *via* Hirshfeld surface analysis and fingerprint plots utilizing Crystal Explorer 3.1 [29]. The Hirshfeld surfaces of compound **2** have been mapped over d_{norm}, shape index, d_e and d_i. All the Hirshfeld surfaces are shown as transparent to allow visualization of compound **2**, around which they were calculated. The distance from the Hirshfeld surface of molecule to the nearest atoms outside and inside the surface are represented as d_i and d_e surfaces, respectively. The normalized contact distance (d_{norm}) based on both d_e and d_i. Red-blue-white color scheme seen in the d_{norm} surface represent shorter contacts, longer contacts and equal contacts around the Van der Waals separation, respectively.

The 2D fingerprint plots from the Hirshfeld surface analysis illustrated the percentage contributions of inter-molecular interactions on the molecules. The contributions to the total Hirshfeld surface of H···H, C···H, O···H and N···H interactions, including reciprocal contacts for all compounds, are observed as 52.2, 32.0, 8.9 and 4.2%, respectively (Figure 5).

Figure 6 displays the Hirshfeld surface of compound **2** mapped over d_{norm} in front and back views and d_{norm} Hirshfeld surface surrounded by one neighboring molecule associated with close contacts of compound **2**.

Table 4. Geometrical parameters of π···π interactions for compounds **2** (Å, °).

Rings I–J [a]	Cg(I)···Cg(J) [b]	γ [c]	Cg(I)-perp [d]	Cg(J)-perp [e]	Symmetry
Cg(1)···Cg(1)	4.523(3)	51.4	2.823(2)	-3.849(2)	-1/2+*x*, -*y*, *z*
Cg(1)···Cg(1)	4.523(3)	31.7	-3.849(2)	2.823(2)	1/2+*x*, -*y* ,*z*
Cg(3)···Cg(3)	4.614(3)	54.3	-2.6953(19)	3.8696(19)	1/2+*x*, 1-*y*, *z*
Cg(3)···Cg(3)	4.613(3)	33.0	3.8693(19)	-2.6949(19)	-1/2+*x*, 1-*y*, *z*
Cg(4)···Cg(3)	4.676(3)	61.4	-2.2416(15)	3.8857(19)	1/2+*x*, 1-*y*, *z*
Cg(4)···Cg(1)	4.597(3)	61.2	2.2161(15)	-3.821(2)	-1/2+*x*, -*y*, *z*
Cg(3)···Cg(3)	4.399(7)	33.2	-3.842(2)	2.688(2)	1/2+*x*, 1-*y*, *z*

[a] Cg(1), Cg(2), Cg(3) and Cg(4) are the centroids of the rings N2-C13-C14-C15-C16, C2-C7,C9-C10-C11-C12-C16 and C9-C15 for compound **2**, respectively.
[b] Centroid distance between ring I and ring J.
[c] Angle between the centroid vector Cg(I)···Cg(J) and the normal to plane J.
[d] Perpendicular distance of Cg(I) on ring J (Å).
[e] Perpendicular distance of Cg(J) on ring I (Å).

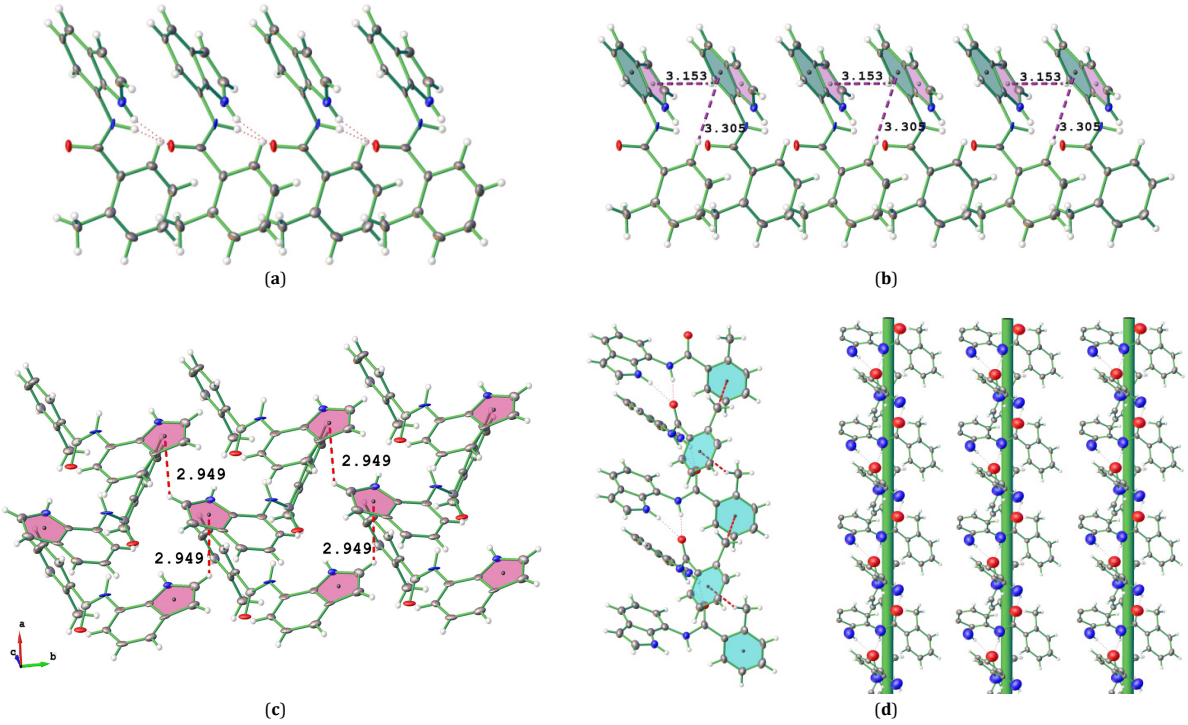

Figure 2. View of the chains along (**a**) the [010] direction resulting from intermolecular N-H···O, (**b**) C-H···π interactions lead to supramolecular chain along the [010], (**c**) [101] direction, (**d**) the helical chain formed via N-H···O and C-H···π (2.86 Å, 1/2+*x*, 1-*y*, *z*) interactions along the [001] direction.

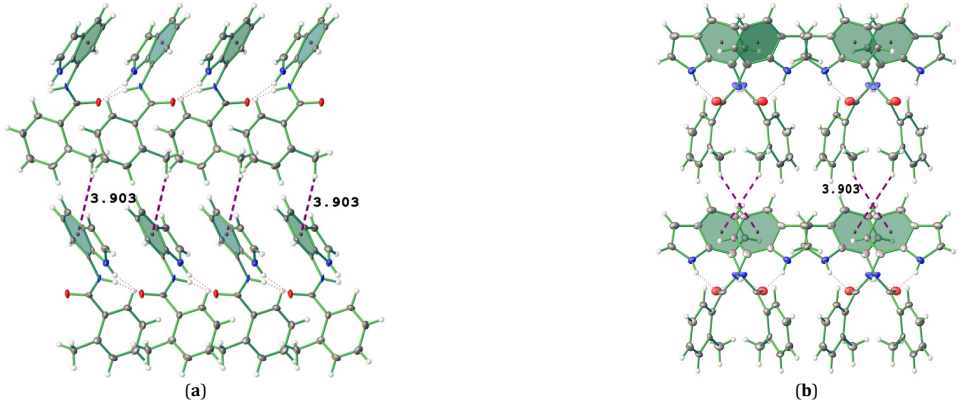

Figure 3. Interconnect of supramolecular chains *via* C-H···π stacking interactions along the (**a**) [010] and (**b**) [001] direction.

The H···O contacts in the Hirshfeld surface mapped over d_{norm} are visible as dark red spots. These contacts represent strong N_{amide}-H···O and N_{indole}-H···O hydrogen bonds and are significant contacts which comprise 8.9% of the total surfaces of each molecule in compound **2**.

The presence of these strong interactions are also indicated through the orange spots present on the Hirshfeld surface mapped over d_i function (shown with red arrows, Figure 7a while the reciprocal contacts of these interactions (O···H-N_{amide} and O···H-N_{indole}) are visible as orange spots on

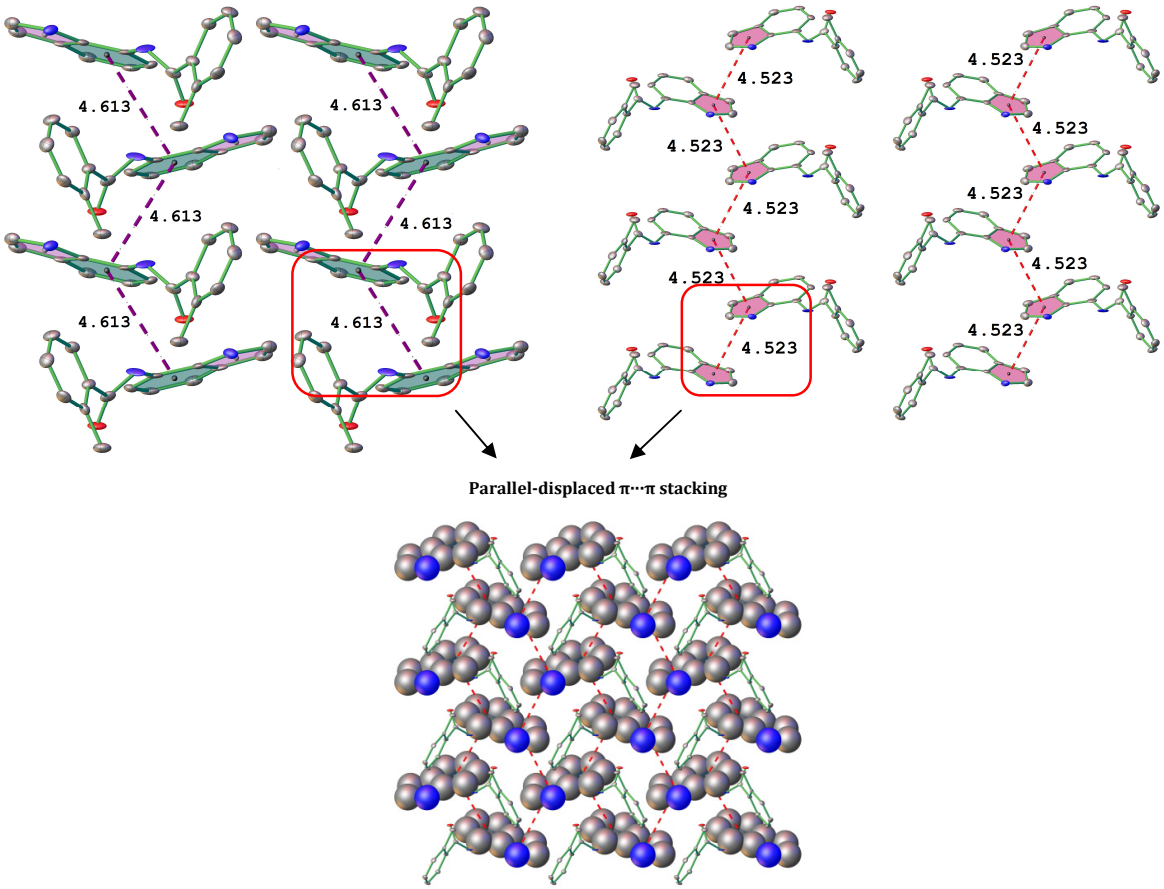

Figure 4. Zigzag chains governed by intermolecular π···π stacking contacts along [001] direction in the crystal structure of compound **2**.

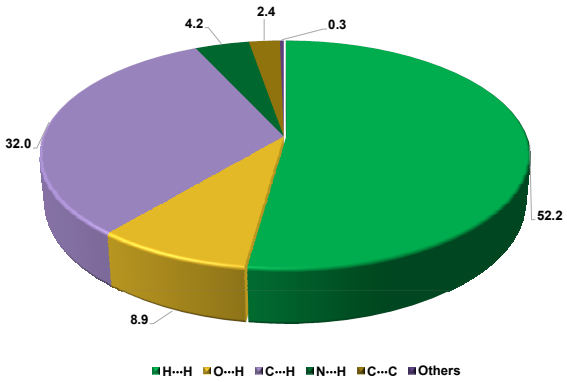

Figure 5. Relative contributions to the percentage of Hirshfeld surface area for the various intermolecular contacts in the compound **2**.

the Hirshfeld surface mapped over d_e function (shown with red arrows, Figure 7b). The other several red spots seen in the d_{norm} surface are due to reciprocal C···H interactions.

C···H/H···C interactions are mainly responsible for the molecular packing in the supramolecular structure with 32.0% contributions to the Hirshfeld surface and they represent C-H···π interactions. These interactions on the Hirshfeld surface mapped with shape index function are appear as hollow orange areas (π···H-C) and bulging blue areas (C-H···π) (Figure 8). These interactions are also seen on the d_e and d_i Hirshfeld surfaces (Figure 7). The strongest of these interactions are indicated through the pale yellow spots present on the d_e and d_i Hirshfeld surfaces. The weak ones of these interactions are seen as blue regions.

The electrostatic deformation density map shows the electron density about one molecule of compound **2** (Figure 9). The deformation density represents a difference between the total electron density of a molecule and the electron density of "neutral spherical unperturbed atoms" superimposed on the same molecule. The electrostatic deformation density map reveals the presence of a charge depletion region (in red) at the H1 which is directed toward the charge concentration region (in blue) over O1 atom, facilitating formation of the N-H···O contacts in the crystal.

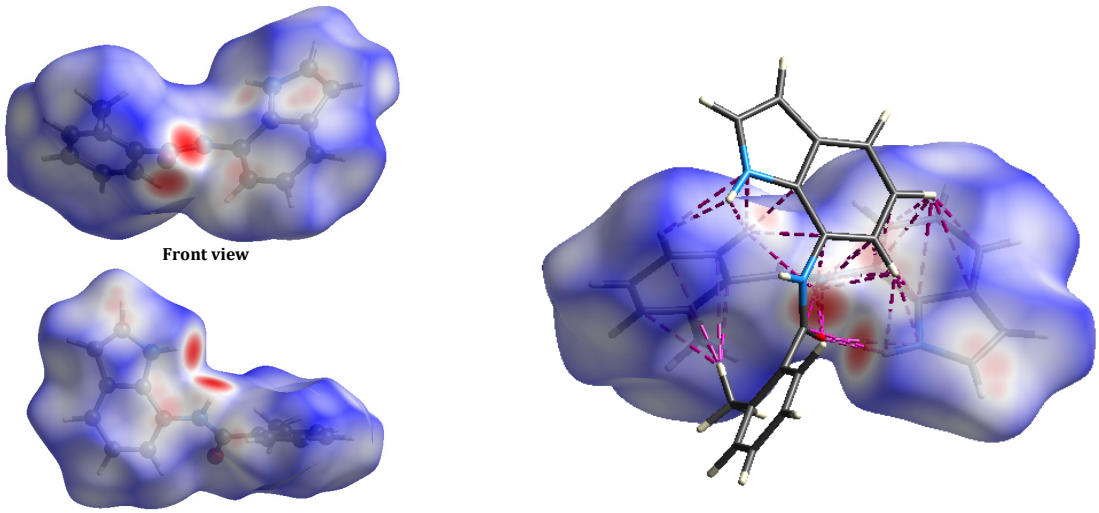

Figure 6. The Hirshfeld surface of compound **2** mapped over d_{norm} (front and back) and d_{norm} Hirshfeld surface surrounded by one neighboring molecule associated with close contacts.

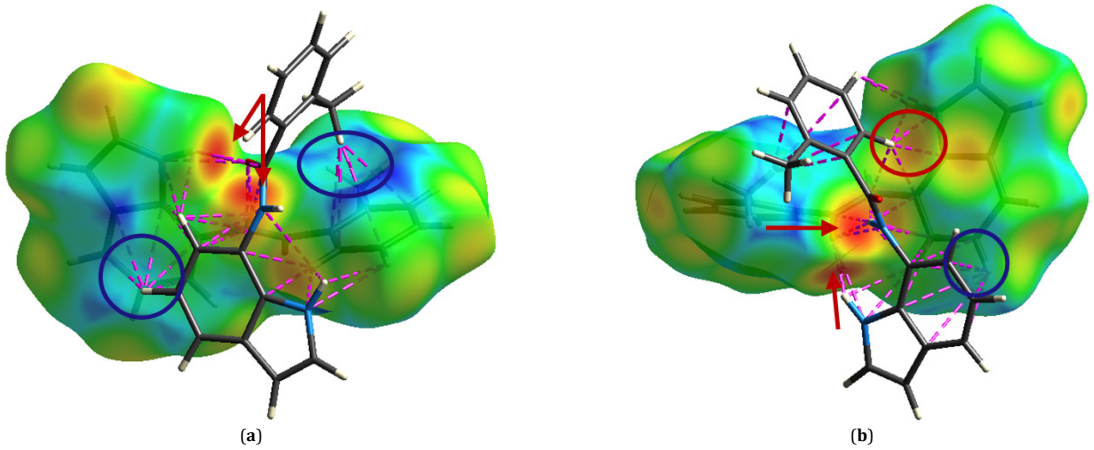

Figure 7. The Hirshfeld surface mapped over the d_i (**a**) and d_e (**b**) with close interactions between two vicinal molecules of compound **2** in the two orientations.

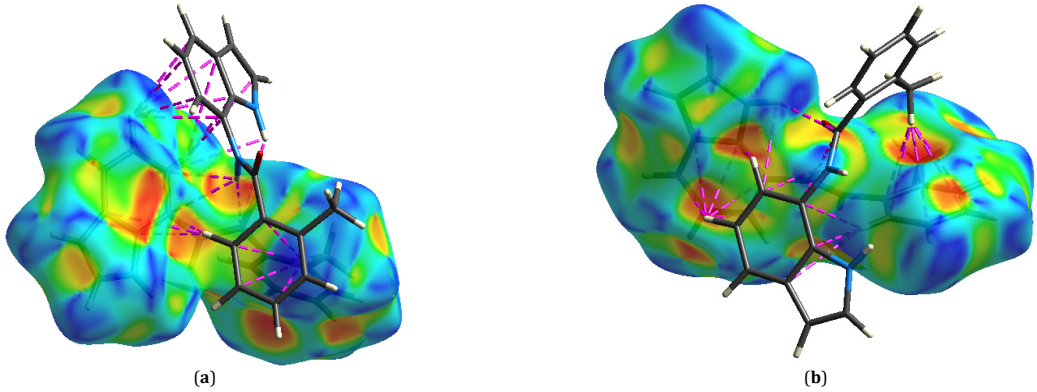

Figure 8. The Hirshfeld surface mapped over the shape index with close interactions between two vicinal molecules of compound **2** in the two orientations.

In the crystal packing of compound **2**, the interactions between the charge depletion and charge concentration regions in the H···O contact provides the overall stabilization in complex structure.

3.4. Antimicrobial activity studies

The *in vitro* biological activity of the compound **2** was tested towards six types of bacteria and two types of fungal.

Table 5. MIC values (μg/mL) of the compound **2** tested against the Gram positive, Gram negative bacteria and fungal [1].

Compound	Gram positive bacteria			Gram negative bacteria			Fungi	
	S. Aureus	*S. Pneumoniae*	*B. Subtilis*	*E. Coli*	*P. Aeruginosa*	*A. Baumannii*	*C. Albicans*	*C. Glabrata*
2	125	125	125	125	125	62.5	62.5	31.25
Flucanozole	-	-	-	-	-	-	*	*
Ampicillin	*	*	*	31.25	*	15.62	-	-

[1] "*": Effective in all concentrations used.

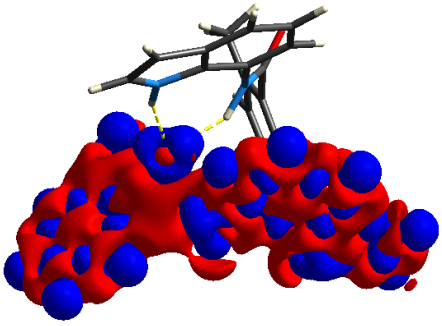

Figure 9. The deformation density map for compound **2** showing the presence of charge depletion regions (in red) and charge concentration regions (in blue).

The organisms used in the present investigations included *S. Aureus, B. Subtilis* and *S. pneumoniae* (as Gram positive bacteria), *E. coli*, *P. aeruginosa* and *A. baumannii* (as Gram negative bacteria) and *C. albicans* and *C. glabrata* (as fungal). The results of the biological activity of the compound **2** was recorded and compared with fluconazole (for fungal) and ampicillin (for bacteria) reference drugs. MIC values are listed in Table 5.

The compound **2** inhibited the growth of bacteria strains with MIC values ranging between 62.5-125 μg/mL. The compound **2** exhibited the highest activities against *A. baumannii* bacterium with MIC values at 62.5 μg/mL. But when the compound **2** compared with ampicillin, which was used as reference drug, it demonstrated lower activity against all the bacteria chains. Similarly, the compound **2** inhibited the growth of fungal strains with MIC values at 31.25 and 62.5 μg/mL but it isn't as effective as fluconazole, which was used as reference drug against all fungal strains. Hence, from all these observations, it was concluded that compound **2** could not be exploited for the design of novel antimicrobial drug.

4. Conclusion

In this study, the compounds named as 1*H*-indole-7-amine (**1**) and *N*-(1*H*-indol-7-yl)-2-methylbenzamide (**2**) were synthesized and structurally characterized by NMR and FT-IR spectroscopic techniques. The molecular structure of compound **2** was also characterized by single-crystal X-ray diffraction technique. According to single crystal X-ray diffraction it was established that the crystal structure of compound **2** is stabilized by intramolecular hydrogen bond of the C-H···O type, formed between the carbonyl oxygen atom and the phenolic ring hydrogen atom or methyl hydrogen atom. In addition, N-H···O, C-H···π and π···π intermolecular interactions play a crucial role for the formation of supramolecular architectures in the structure of compound **2**. These intermolecular contacts in compound **2** have been also examined based on the Hirshfeld surfaces and their associated 2D fingerprint plots. Furthermore, compound **2** was evaluated for both, their *in-vitro* antibacterial and antifungal activity.

Acknowledgement

This work was supported by Mersin University Research Fund [Project No: 2015-AP4-1162].

Supplementary material

Crystallographic data for the structure reported in this paper have been deposited at the Cambridge Crystallographic Data Centre (CCDC) with quotation number CCDC-1579495 for *N*-(1*H*-indol-7-yl)-2-methylbenzamide and can be obtained free of charge on application to CCDC 12 Union Road, Cambridge CB2 1EZ, UK [Fax: (internat.) +44(1223)336-033, E-mail: deposit@ccdc.cam.ac.uk].

References

[1]. Barluenga, J.; Valdes, C. *Mod. Heterocycl. Chem.* **2011**, *1*, 377-531.
[2]. Chadha, N.; Silakari, O. *Eur. J. Med. Chem.* **2017**, *134*, 159-184.
[3]. Baeyer, A.; Emmerling, A. *Ber. Dtsch. Chem. Ges.* **1869**, *2*, 679-682.
[4]. Joule, J. A. 'Indoles' in 'Science of Synthesis'; Thomas, E. J., Ed.; Georg Thieme: Stuttgart, New York, 2011; Vol. 10 Knowledge Update 2010/2, pp. 526.
[5]. Faulkner, D. *J. Nat. Prod. Rep.* **2001**, *18*, 1-49.
[6]. Chelucci, G. *Coord. Chem. Rev.* **2017**, *331*, 37-53.
[7]. Sharma, V.; Kumar, P.; Pathak, D. *J. Heterocycl. Chem.* **2010**, *47*, 491-502.
[8]. Kaushik, N. K.; Kaushik, N.; Attri, P.; Kumar, N.; Kim, C. H.; Verma, A. K.; Choi, E. H. *Molecules* **2013**, *18*, 6620-6662.
[9]. Suzen, S.; Buyukbingol, E. *Il Farmaco* **2000**, *55*, 246-248.
[10]. Buyukbingol, E.; Suzen, S.; Klopman, G. *Il Farmaco* **1994**, *49*, 443-447.
[11]. Pojarova, M.; Kaufmann, D.; Gastpar, R.; Nishino, T.; Reszka, P.; Bednarskib, P. J.; Angerer, E. V. *Med. Chem.* **2007**, *15*, 7368-7379.
[12]. Morteza, S.; Mohammad, A. Z.; Hendrik, G. K.; Zahra, T. *Chem. Rev.* **2010**, *110*, 2250-2293.
[13]. Chyan, Y. J.; Poeggler, B.; Omar, R. A.; Chain, D. G.; Frangione, B.; Ghiso, J.; Pappolla, M. A. *J. Biol. Chem.* **1999**, *274*, 21937-21942.
[14]. Suzen, S.; Buyukbingol, E. *Il Farmaco* **1998**, *53*, 525-527.
[15]. Darehkordi, A.; Rahmani, F.; Hashemi V. *Tetrahedron Lett.* **2013**, *54*, 4689-4692.
[16]. Srivastava, N.; Banik, B. K. *J. Org. Chem.* **2003**, *68*, 2109-2114.
[17]. Shimazakia, Y.; Yajimab, T.; Takanic, M.; Yamauchi, O. *Coord. Chem. Rev.* **2009**, *253*, 479-492.
[18]. Kordic, B.; Kovacevic, M.; Sloboda, T.; Vidovic A.; Jovic, B. *J. Mol. Struct.* **2017**, *1144*, 159-165.
[19]. Nocek, J. M.; Zhou, J. S.; De Forest, S.; Priyadarshy, S.; Beratan, D. N.; Onuchic, J. N.; Hoffman, B. M. *Chem. Rev.* **1996**, *96*, 2459-2489.
[20]. Dougherty, D. A. *Science* **1996**, *271*, 163-168.
[21]. Ma, J. C.; Dougherty, D. A. *Chem. Rev.* **1997**, *97*, 1303-1324.
[22]. Gallivan, J. P.; Dougherty, D. A. *Proc. Natl. Acad. Sci. USA* **1999**, *96*, 9459-9464.
[23]. Dolomanov, O. V.; Bourhis, L. J.; Gildea, R. J.; Howard, J. A. K.; Puschmann, H. *J. Appl. Cryst.* **2009**, *42*, 339-341.
[24]. Palatinus, L.; Chapuis, G. *J. Appl. Cryst.* **2007**, *40*, 786-790.
[25]. Palatinus, L.; VanderLee, A. *J. Appl. Cryst.* **2008**, *41*, 975-984.
[26]. Palatinus, L.; Prathapa, S. J.; VanSmaalen, S. *J. Appl. Cryst.* **2012**, *45*, 575-580.

[27]. Sheldrick, G. M. *Acta Cryst. C* **2015**, *71*, 3-8.
[28]. Zielinski, T.; Dydio, P.; Jurczak, J. *Tetrahedron* **2008**, *64*, 568-574.
[29]. Turner, M. J.; McKinnon, J. J.; Wolff, S. K.; Grimwood, D. J.; Spackman, P. R.; Jayatilaka, D.; Spackman, M. A. CrystalExplorer17, University of Western Australia, 2017.
[30]. Burlesson, F. G.; Chambers, T. M.; Wedbrauk, D. L. Virology. A Laboratory Manual, Academic Press, New York, 1992.
[31]. National Committee for Clinical Laboratory Standards. Reference method for broth dilution antifungal susceptibility testing of yeasts. Approved standard NCCLS document M27-A. National Committee for Clinical Laboratory Standards, Wayne, Pa., (2002).
[32]. Arslan, H.; Duran, N.; Borekci, G.; Ozer, C. K.; Akbay, C. *Molecules* **2009**, *14*, 519-527.
[33]. Planas J. G.; Masalles, C.; Sillanpa, R.; Kivekas, R.; Teixidor, F.; Vinas, C. *Cryst. Eng. Comm.* **2006**, *8*, 75-83.